RSC Advances

PAPER

View Article Online
View Journal | View Issue

Cite this: *RSC Adv.*, 2023, **13**, 29152

Dipeptide-1 modified nanostructured lipid carrier-based hydrogel with enhanced skin retention and topical efficacy of curcumin

Ming Yuan, † Jiangxiu Niu,† Fei Li, Huiyuan Ya,* Xianghui Liu, Keying Li, Yanli Fan and Qiuyan Zhang

Topical administration of curcumin (CUR), a natural polyphenol with potent anti-inflammation and analgesic activities, provides a potential approach for local skin diseases. However, the drug delivery efficiency is highly limited by skin barriers and poor bioavailability of CUR. Herein, we propose hydrogel containing CUR-encapsulated dipeptide-1-modified nanostructured lipid carriers (CUR–DP–NLCs gel) to enhance topical drug delivery, and improve the topical therapeutic effect. The prepared CUR–DP–NLCs were characterized and were suitably dispersed into the Pluronic F127 hydrogel for topical application. The optimized CUR–DP–NLCs had a particle size of 152.6 ± 3.47 nm, a zeta potential of −33.1 ± 1.46 mV, an entrapment efficiency of 99.83 ± 0.14%, and a spherical morphology. X-ray diffraction (XRD) studies confirmed that CUR was successfully entrapped by the NLCs in an amorphous form. CUR–DP–NLCs gel exhibited sustained release over 48 h and significantly increased the skin retention of CUR. *In vitro* skin retention of CUR with CUR–DP–NLCs gel was 2.14 and 2.85 times higher than that of unmodified NLCs gel and free CUR, respectively. Fluorescence microscopy imaging revealed the formed nanoparticles accumulated in the hair follicles with prolonged retention time to form a drug reservoir. The hematoxylin–eosin staining showed that CUR–DP–NLCs gel could change the microstructure of skin layers and disturb the skin barriers. After topical administration to mice, CUR–DP–NLCs gel showed better analgesic and anti-inflammatory activities with no potentially hazardous skin irritation. These results concluded that CUR–DP–NLCs gel is a promising strategy to increase topical drug delivery of CUR in the treatment of local skin diseases.

Received 14th July 2023
Accepted 11th September 2023

DOI: 10.1039/d3ra04739c

rsc.li/rsc-advances

1. Introduction

Curcumin (CUR), a natural polyphenol derived from the rhizome of *Curcuma longa* L., is known for its analgesic, anti-inflammatory, anti-cancer, antimicrobial and anti-oxidant properties.[1,2] Recently, an increasing amount of evidence has suggested that CUR may represent an effective agent in the treatment of several skin diseases, such as psoriasis, atopic dermatitis, iatrogenic dermatitis, and skin infections.[3] For these skin diseases, topical application is more effective to deliver CUR to the skin for local therapy. However, CUR has poor bioavailability due to its low stability, low water solubility, and rapid metabolism, all of which hinder it from being developed as a therapeutic agent.[4,5] In addition, the tight junctions of corneocytes and lipid matrix in the stratum corneum impose a significant barrier for percutaneous delivery of CUR.[6] Thus, there is a need to develop new CUR formulations to promote its percutaneous absorption and prolong its retention time at the site of action, so as to enhance the local treatment effect.

Nanoparticle-based drug delivery systems have been increasingly exploited to encapsulate and deliver CUR, including liposomes, nanoemulsions, polymeric micelles and lipid nanoparticles.[7–9] Nanostructured lipid carrier (NLC), an advanced and second-generation lipid colloidal system, is mainly composed of solid lipid, liquid lipid and surfactants.[10] Because the crystal of solid lipid is disrupted by liquid lipid to form a lattice defects, NLC has an imperfect lipid matrix that offers more space for drug entrapment and prevents drug expulsion during storage.[11,12] As an effective topical delivery system, the nanosized NLC particles can tightly adhere to the skin surface and exhibit occlusion effect, which improve skin hydration and promote the penetration of drugs.[13–15] In addition, the lipids and surfactants used in NLC can also function as permeation enhancers by disrupting the skin barriers through loosening and fluidization of the lipid bilayers in stratum corneum.[16] However, NLC dispersion exhibits strong fluidity and is inconvenient to use on the skin. Hydrogel shows appropriate viscosity and ductility as well as good biocompatible on the skin, exhibiting great potential in biomedical engineering.[17,18]

College of Food and Drug, Luoyang Normal University, Luoyang, Henan 471934, People's Republic of China. E-mail: yahuiyuan@lynu.edu.cn

† Ming Yuan and Jiangxiu Niu contributed equally to this work.

Consequently, the immobilization of NLC into hydrogel matrix can improve applicability and prolong residence time on the skin.

Acetyl dipeptide-1 cetyl ester (*N*-acetyl-L-tyrosyl-L-arginine hexadecyl ester), a derivate of the bioactive dipeptide tyrosyl-arginine, is the most used ingredient in cosmetic products for sensitive skin.[19] It can penetrate the stratum corneum and retain in the skin to reduce stinging sensation and inflammation processes. Acetyl dipeptide-1 cetyl ester could promote the pro-opiomelanocortin (POMC) expression, which facilitating the release of the opioid met-enkephalin, as well as reducing the release of the calcitonin gene related peptide (CGRP). CGRP could activate transient receptor potential vanilloid type 1 (TRPV1) in cutaneous nerve fibres and keratinocytes, thus initiating an inflammatory response.[20] Furthermore, it has been shown to significantly reduce prostaglandin E2 (PGE_2) secretion and decrease nuclear factor κB (NFκB) signalling, which is associated with neurogenic inflammation in sensitive skin.[21] Consequently, it could be concluded that acetyl dipeptide-1 cetyl ester might be an effective ingredient to reduce inflammatory responses and painful sensations in skins.

In the present study, we aimed to develop acetyl dipeptide-1 cetyl ester-modified nanostructured lipid carriers (CUR–DP–NLCs) as potential carriers for the topical delivery of CUR (Fig. 1). The CUR–DP–NLCs, combining the advantages of NLC nanoparticles and acetyl dipeptide-1 cetyl ester, exerted localizing effect in skin with retention of drug in epidermis and dermis layers resulting in higher therapeutic efficacy against local skin inflammation. Then the optimized CUR–DP–NLCs were dispersed into Pluronic F127 (F127)-based thermoresponsive hydrogel, which existed as a liquid at low temperature and as a semisolid gel at high temperature. The hydrogel showed appropriate viscosity and ductility allowing high local nanoparticle concentrations to be maintained at the skin surface. The CUR–DP–NLCs gel was assessed for physicochemical properties, then *in vitro* skin permeation and retention, *in vivo* anti-inflammatory and analgesic activity, and skin irritation were further investigated.

2. Materials and methods

2.1. Materials

Glyceryl monostearate (GMS) was obtained from Shandong Usolf Chemical Technology Co., LTD (Shandong, China). Poloxamer 188 (F-68), Pluronic F127, caprylic/capric triglyceride (GTCC) and soybean phospholipids (SPC) were purchased from BASF (Shanghai, China). Curcumin was purchased from Xi'an Ivy Biotechnology Co. Ltd (Xian, China). Acetyl dipeptide-1 cetyl ester was provided by Go Top Peptide Biotech Co., Ltd. (Hangzhou, China). All other chemicals and reagents were at least of analytical reagent grade.

2.2. Animals

Female ICR mice (18–22 g weight) and Sprague-Dawley (SD) rats (180–220 g weight) were procured from the Henan Experimental Animal Center (Zhengzhou, China). The animals were acclimatised at regulated temperature (20 ± 5 °C) and humidity (50 ± 5%) under natural light/dark conditions for at least 1 week before experimentation, fed with a standard diet and allowed water *ad libitum*. The experimental protocols were in accordance with the guidelines approved by Luoyang Normal

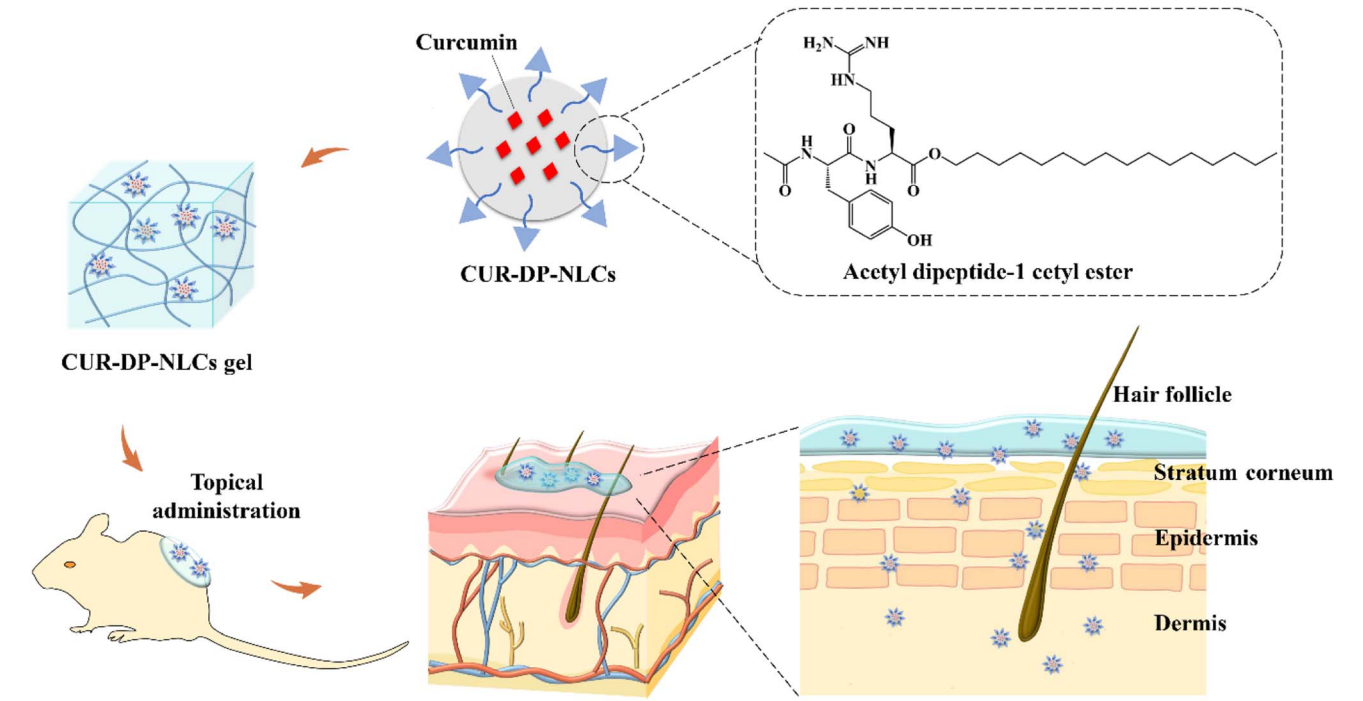

Fig. 1 Schematic illustration of preparation and application of CUR–DP–NLCs gel. The generated CUR–DP–NLCs gel was painted locally and exhibited enhanced skin retention effect.

University, and the study was approved by the Experimental Animal Ethics Committee.

2.3. Preparation and optimization of CUR–DP–NLCs

CUR–DP–NLCs were prepared by the emulsion evaporation and low temperature-solidification method.[22] Briefly, GTCC (320 mg), SPC (300 mg), GMS (640 mg), CUR (15 mg), and acetyl dipeptide-1 cetyl ester (0, 10, 20, 30, 40 mg of acetyl dipeptide-1 cetyl ester was added separately to optimize the best amount in the formulation) were dissolved in 5 mL ethanol at 75 °C to get the oil phase. And then the oil phase was injected into 15 mL of aqueous solution containing 300 mg of F-68 (heated at 75 °C) under high-speed homogenization (T25, IKA, Germany) of 10 000 rpm for 15 min to get a homogeneous emulsion. The resulting emulsion was kept stirring for 1 h at 75 °C to evaporate ethanol. Then the nanoemulsion was dispersed rapidly into 15 mL of deionized water (0 °C) in an ice bath with stirring (1000 rpm) for 30 min. Finally, the CUR–DP–NLCs were obtained and stored in 4 °C for further research. The preparation method of CUR loaded NLCs without acetyl dipeptide-1 cetyl ester (CUR–NLCs) was similar to that described above. Hydrogel containing NLC nanoparticles (CUR–DP–NLCs gel) was prepared by a slow dispersion under magnetic stirring of Pluronic F127 powder (20 wt%) directly into NLC suspension at 4 °C until complete dissolution of the powder.

2.4. Characterization of the formulation

2.4.1 Particle size and zeta potential measurement. The particle size, polydispersity index (PDI) and zeta potential of CUR–DP–NLCs were evaluated by dynamic light scattering (DLS) using Malvern Nano ZS 90 (Malvern, UK). All the samples were diluted with deionized water to get a suitable concentration for examination and every sample was measured in triplicate.

2.4.2 Entrapment efficiency (EE) determination. EE was evaluated according to the ultrafiltration-centrifugation method.[23] 1 mL of the CUR–DP–NLCs dispersion was added in an ultrafiltration centrifuge tube (Amicon Ultra 30 kDa, Millipore, Germany) and centrifuged at 5000 rpm for 10 min. The filtrate was diluted with ethanol and the amount of unencapsulated CUR was quantified by an UV-vis spectrophotometry method at 425 nm (TU-1810PC, Purkinje, Beijing, China). The EE% was calculated according to the following equation:

$$\mathrm{EE}\% = \left[\frac{\text{total amount of drug} - \text{unencapsulated amount of drug}}{\text{total amount of drug}}\right] \times 100$$

All measurements were performed in triplicate and the results were reported as mean values ± standard deviation (SD) of three replicates ($n = 3$).

2.4.3 Morphology analysis. The surface morphologies of CUR–DP–NLCs and CUR–DP–NLCs gel were observed by scanning electron microscope (SEM) (Sigma 500, ZEISS, Germany). Diluted suspension of CUR–DP–NLCs was dropped onto a silicon substrate and dried overnight at room temperature. The lyophilized CUR–DP–NLCs gel was placed on the conductive tape. Both the samples were coated with gold under vacuum, and then imaged with an accelerating voltage of 3–5 kV.

2.4.4 Rheological analyses. Changes of the rheological properties of CUR–DP–NLCs gel with the temperature were investigated using a rotational rheometer (Kinexus Ultra+, Netzsch, Germany). The hydrogel was placed between the parallel plates with a gap of 1 mm. The temperature sweep analysis was carried out over the range of 4–60 °C and a rate of 2 °C min^{-1}, followed by keeping the strain and frequency constant as 1% and 1 Hz, respectively.

2.4.5 X-ray diffraction (XRD). The XRD patterns of CUR, physical mixture of drug and excipients, lyophilized blank DP–NLCs gel, and lyophilized CUR–DP–NLCs gel were obtained using an X-ray diffractometer (D8 Advance, Bruker, Germany) employed with Cu-Kα radiation at 40 kV and 40 mA. The measurements were performed at room temperature, scanning at 2θ from 5° to 50° with a 0.02° step size.

2.4.6 *In vitro* drug release. *In vitro* release studies were performed by dialysis method using a cellulose membrane of MWCO 8–14 kDa.[24] PBS (pH 7.4) with 1% Tween-80 (40 mL) was selected as release medium. CUR solution, CUR–NLCs, CUR–DP–NLCs, CUR–NLCs gel and CUR–DP–NLCs gel (equivalent to 1 mg of CUR) were added into the dialysis bags, followed by submerging into the release medium (37 ± 0.5 °C), and were incubated in a shaking bath at 100 rpm. At predetermined time intervals (1 h, 2 h, 4 h, 8 h, 12 h, 24 h, 36 h, and 48 h), 1 mL of the release medium was sampled and replaced with 1 mL of fresh medium. The content of CUR was monitored by UV-vis spectrophotometer at 425 nm, and all experiments were repeated three times and the results were expressed as mean ± SD.

2.5. *In vitro* skin permeation and retention studies

The permeation studies were performed utilizing a Franz diffusion cell apparatus (RYJ-6B, Shanghai Huanghai Drug Control Instrument Co., Ltd, China). The full-thickness skin obtained from the shaved dorsal region of SD rats was removed, freed from any subcutaneous adipose tissue, and inspected carefully to assure uniform thickness and integrity of the skin. The skin samples were positioned between the donor and acceptor chamber (the dermal side contacted directly to the donor medium) with effective diffusion area of 2.8 cm^2 and a cell volume of 6.5 mL. The receptor medium was PBS (pH = 7.4) with 1% Tween-80 to meet sink conditions. The acceptor chamber was kept at 37 ± 0.5 °C and stirred at 300 rpm. Subsequently, CUR–DP–NLCs gel, CUR–NLCs gel and CUR

solution (equivalent to 0.15 mg of CUR) were applied onto the skins. At predefined time intervals (2, 4, 6, 8, 10, 12, 24 h), 1 mL of the receptor medium was withdrawn and substituted with fresh receptor medium. The amount of CUR permeates the skin was determined using an HPLC instrument (U-3000, Thermo, USA) with a C18 column (5 mm, 200 × 4.6 mm; Wondasil, Japan). The composition of the mobile phase was acetonitrile: 0.5% phosphoric acid water (58 : 42, v/v), the flow rate was set at 1 mL min^{-1}, and the column oven temperature was set at 30 °C. Samples were inspected at a detection wavelength of 423 nm. The patterns of the permeation of CUR were created *via* plotting the cumulative amount of CUR permeated through unit area *versus* time.

To perform the skin retention test, after finishing the *in vitro* permeation study the skin samples were removed and cleaned. Then the skin samples were respectively cut into pieces with scissor and immersed in 2 mL methanol for 24 h at 4 °C, subsequently placed in an ultrasound bath (KQ-250DE, Kunshan, China) for 3 h. Then it was refrigerated centrifuged at 10 000 rpm for 10 min and the supernatant was filtered by a syringe with a Millipore filter (0.22 μm).[7,25] The filtrate was analysed using the same HPLC method described above, and the cumulative amount of CUR retained in the skin per unit area was calculated.

2.6. *In vivo* fluorescence imaging analysis

ICR mice in similar development stages were randomly divided into 3 groups, and the dorsal hair of the mice was carefully shaved the day before the experiment while avoiding damage to stratum corneum. To visualize the permeation, CUR–DP–NLCs gel, CUR–NLCs gel and CUR solution with the same amount of CUR (0.1 mg) were evenly spread on a 1 cm^2 shaved dorsal skin. At 1 h and 6 h after the treatment period, the application sites were cleaned by physiological saline to eliminate any material remaining in the surface. Subsequently the mice were humanely sacrificed, and skin samples were collected. The skin tissues were frozen at −80 °C and vertically sliced by a freezing slicer (CM1950, Leica, Germany). The skin sections were nucleus counterstained with 4′,6-diamidino-2-phenylindole (DAPI) and visualized by an automatic digital slide scanner (CUR Ex/Em = 425/515 nm, Pannoramic MIDI, 3DHISTECH, Hungary).

2.7. Histological analysis

To investigate the effect of the formulations on skin microstructure, histological sectioning and HE staining was performed.[26] ICR mice were randomly divided into 4 groups, and the dorsal hair of the mice was carefully shaved 24 h before the experiment. CUR–DP–NLCs gel, CUR–NLCs gel, CUR solution and physiological saline were applied to an area of approximately 1 cm^2 on the naked dorsal skins for 6 h. The mice were then sacrificed and the skin samples were carefully dissected. The skin samples were rinsed with physiological saline, fixed in 4% paraformaldehyde, and processed for paraffin inclusion. The paraffin blocks were cut into longitudinal sections of 5 μm thickness, stained with HE, and then observed for histological analysis by an automatic digital slide scanner (Pannoramic MIDI, 3DHISTECH, Hungary).

2.8. *In vivo* hot plate test

The analgesic activity was determined in mice using hot plate method.[27] Mice were placed on an intelligent hot plate apparatus (YLS-6B, Jinan, China) kept at a temperature of 55 ± 0.5 °C. The mice were randomly divided into five groups, which were respectively treated on the planta with 0.4 g of CUR–DP–NLCs gel, CUR–NLCs gel, CUR solution (containing 0.4 mg CUR), blank F127 gel and normal saline for 30 min. The reaction time was determined as the time taken for the mice to response to the thermal pain by licking their hind paws. The reaction time was recorded before and 30, 60, 120 min after the topical application of each formulation ($n = 8$ for each group). The cut-off time was fixed at 60 s in order to avoid animal tissue damage.

2.9. Xylene-induced ear edema test

The anti-inflammatory activity of the developed formulations was investigated by using model of xylene-induced ear edema in mice according to the reported method.[28] The mice were randomly divided into five groups, 8 in each group. CUR–DP–NLCs gel, CUR–NLCs gel, CUR solution (containing 0.1 mg CUR, respectively), blank F127 gel and normal saline were topically administered to both sides of the right ear of the mice. One hour after treatment, 30 μL of xylene was applied on the inner and outer surface of the right ear while the left ear served as control. After 30 min, the mice were humanely sacrificed and both ears were removed. Circular sections were taken from the ears using a stainless-steel punch with a diameter of 8 mm and weighed. The extent of ear edema expressed as the weight difference between the right and the left ear sections of the same animal. The anti-inflammatory activity was expressed as percentage of the inhibition of ear edema, which was calculated by the following formula:

$$\text{Ear edema inhibition}(\%) = \frac{\text{mean edema of saline group} - \text{mean edema of treated group}}{\text{mean edema of saline group}} \times 100$$

2.10. Skin irritation studies

The skin irritation potential of the developed formulations was assessed in mice according to the previous studies with a few modifications.[29] The dorsal hair of the mice (approximately 2 cm × 2 cm) was carefully shaved without causing tissue damage 24 h before the experiment and randomized into 3 groups ($n = 6$). 0.5 g of CUR–DP–NLCs gel, CUR–NLCs gel and normal saline

(control) were respectively spread on the dorsal regions of the mice. At 4 h after administration, residual samples were removed with warm water. All the mice were visually examined and photographed to validate the degree of irritation at 1, 4, 24, 48 and 72 h. Reactions were graded as negative, mild (erythema alone), moderate (erythema with edema), or severe (erythema, edema, and vesiculation).

2.11. Statistical analysis

All the quantitative experiments were performed at least in triplicate. Data were expressed as the mean values ± SD. The statistical differences between two groups were calculated by Student's *t*-test. *P*-Values < 0.05 were regarded statistically significant.

3. Results and discussion

3.1. Optimization of CUR–DP–NLCs

Acetyl dipeptide-1 cetyl ester is the INCI name for the peptide *N*-acetyl-L-tyrosyl-L-arginine hexadecyl ester. In the preparation of CUR–DP–NLCs, the hexadecyl of acetyl dipeptide-1 cetyl ester could be inserted into the lipid matrix, while the dipeptide Tyr–Arg was exposed on the surface of the NLCs. The optimal amount of acetyl dipeptide-1 cetyl ester used in the formulation was determined, because the insertion of excessive hexadecyl into the lipid matrix might lead to instability of the particles, appeared in the abnormal change of the particle size and PDI. Table 1 showed the changes of these properties with the amount of acetyl dipeptide-1 cetyl ester added in the formulation. When the amount of acetyl dipeptide-1 cetyl ester exceeded 20 mg, the particle size of CUR–DP–NLCs markedly increased, and the particle size distribution was wide with a PDI > 0.5. Furthermore, the EE of different formulations were above 99%, which was attributed to the hydrophobicity of CUR. Therefore, the optimal amount of acetyl dipeptide-1 cetyl ester was determined as 20 mg.

3.2. Characterization of CUR–DP–NLCs

Small particle size allowed for a closer contact with the stratum corneum, and it was reported that nanoparticles smaller than 300 nm were able to deliver the contents to some extent into deep layers of the skin.[30,31] As shown in Table 1, the particle size of optimized CUR–DP–NLCs was 152.6 ± 3.47 nm, which was suitable for skin application. The PDI value was 0.31 ± 0.04, indicating a narrow size distribution and good physical stability. Zeta potential could also be used as a stability predictor of the system. In this study, the optimized CUR–DP–NLCs were negatively charged with zeta potential value of −33.1 ± 1.46 mV. The negative potential in the aqueous test solution was most likely due to the adsorption of the hydroxyl ions on the soy lecithin lipid chains.[32] The colloidal particles exhibiting relatively high surface charge (>30 mV) could repel each other and reduce the aggregation opportunity, thus increase the stability of the system.[33] Moreover, the negatively charged lipids present in the skin and the anionic nanoparticles created a repulsive force, generating temporary channels that could facilitate deeper skin penetration.[30] High EE was an essential prerequisite for effective delivery of drugs at the target site, and the EE of CUR–DP–NLCs reached up to 99.83 ± 0.14%, which exhibited good drug encapsulation ability. Considering the particle size, PDI and EE, CUR–DP–NLCs showed excellent physical properties for topical drug delivery.

3.3. Rheological property of CUR–DP–NLCs gel

Thermoresponsive systems applied to the skin should have a sol–gel transition between 25.0 and 37 °C. Under these conditions, the formulations behave as a liquid at room temperature and as a gel at body temperature, ensuring greater permanence of the formulation at the action site and guaranteeing a higher diffusion drug rate through the skin.[34] The gelation temperature of CUR–DP–NLCs gel was determined by rheology measurements. Fig. 2A illustrated the storage modulus (G') and loss modulus (G'') of CUR–DP–NLCs gel as the temperature changed from 4 to 60 °C. At low temperatures, the G' was lower than the G'', suggesting that the sample remained in the solution with low viscosity. The G' and G'' values were increased rapidly with the increase in temperature due to the sol–gel transition, and the transition temperature of CUR–DP–NLCs gel was 28.19 ± 0.1 °C (sol–gel transition temperature was defined as the intersection of G' and G'' curves during temperature increase[35]). Above sol–gel transition temperature, the G' was significantly higher than the G'', suggesting the hydrogel formation. The observed gelation temperature favored the skin application. At the physiological temperature (around 37 °C), the CUR–DP–NLCs gel would be in the gel phase upon contact with the skin, remaining at the application site (Fig. 2B).

3.4. Surface morphology

The morphologies of the CUR–DP–NLCs and CUR–DP–NLCs gel were observed through SEM (Fig. 2C). The CUR–DP–NLCs were

Table 1 Optimization of the CUR–DP–NLCs formulation

Amount of acetyl dipeptide-1 cetyl ester (mg)	Particle size (nm)	PDI	Zeta potential (mV)	EE (%)
0	109.4 ± 1.40	0.28 ± 0.01	−36.8 ± 2.25	99.87 ± 0.11
10	143.8 ± 0.95	0.21 ± 0.01	−33.5 ± 1.00	99.67 ± 0.08
20	152.6 ± 3.47	0.31 ± 0.04	−33.1 ± 1.46	99.83 ± 0.14
30	268.4 ± 15.08	0.53 ± 0.08	−32.0 ± 0.10	99.93 ± 0.17
40	261.5 ± 5.56	0.55 ± 0.09	−31.0 ± 0.31	99.84 ± 0.12

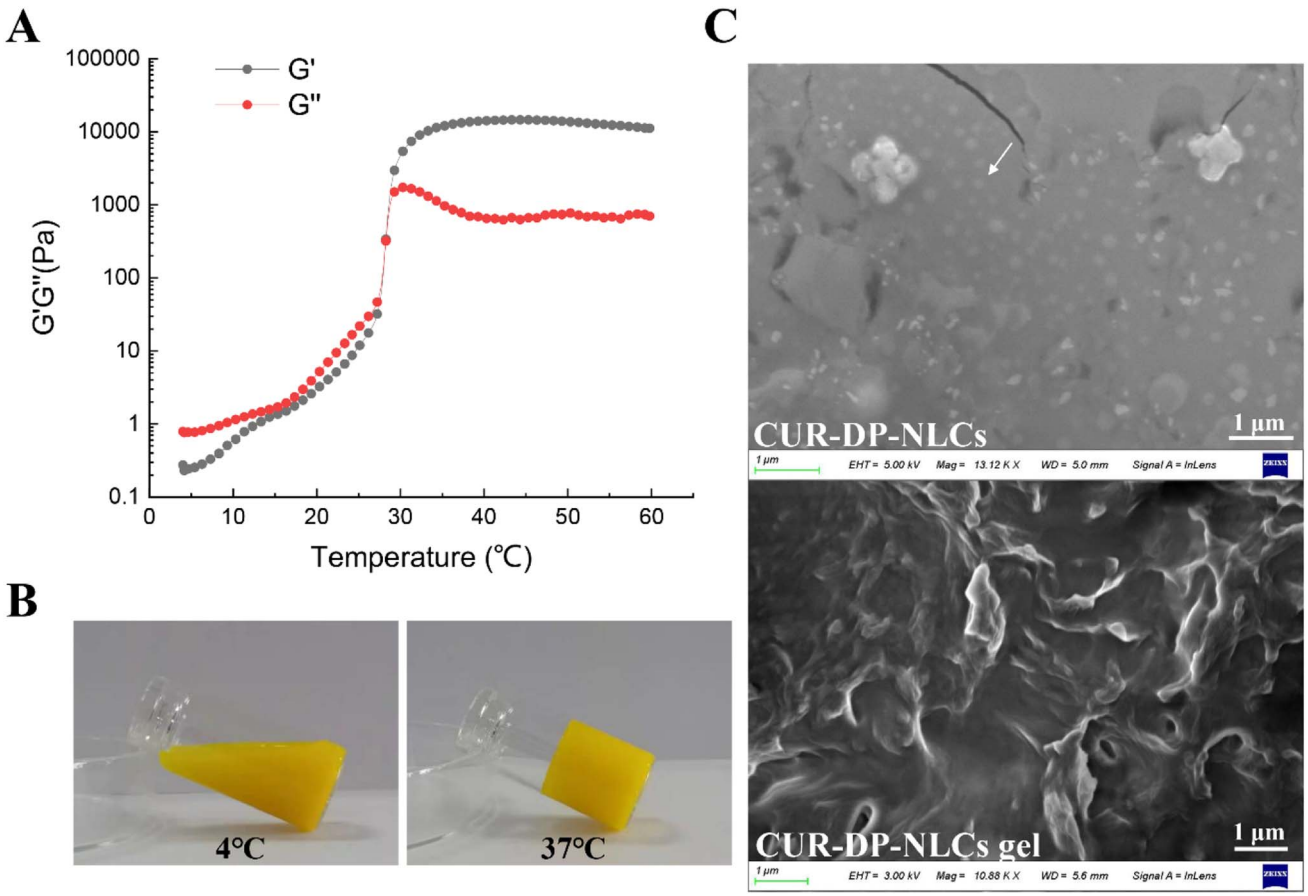

Fig. 2 (A) *G′* and *G″ versus* temperatures from 4 to 60 °C; (B) optical pictures showing the sol–gel transition of CUR–DP–NLCs gel; (C) SEM micrographs of CUR–DP–NLCs and CUR–DP–NLCs gel.

typically spherical with a uniform size and dispersion, which was in accordance with the DLS results. The lyophilized CUR–DP–NLCs gel displayed a typical three-dimensional (3D) porous morphology and the NLC did not affect the pore structure.

3.5. Crystalline properties

The diffractograms of CUR, physical mixture of drug and excipients, lyophilized blank DP–NLCs gel, and lyophilized CUR–DP–NLCs gel were shown in Fig. 3. The XRD spectrum of CUR showed multiple sharp peaks suggesting its crystalline nature. The characteristic peaks of CUR were absent in the XRD spectrum of CUR–DP–NLCs gel, which indicated that CUR was solubilized within the lipid matrix of NLCs and stabilized in an amorphous form.[36] In addition, the spectrum of CUR–DP–NLCs gel was quite similar to that of blank DP–NLCs gel, indicating that the addition of CUR did not change the nature of NLCs. An explanation to this was that the CUR was entrapped in the lipid core of NLCs.[37]

3.6. *In vitro* drug release

The *in vitro* release profiles of CUR from various formulations were shown in Fig. 4. The CUR solution exhibited rapid release and over 80% of drug was released within 12 h. By contrast, CUR–DP–NLCs and non-modified NLCs (CUR–NLCs) presented a biphasic drug-release pattern (an initial burst release in the first 12 hours, followed by a slow, sustained release of up to 48 h). The burst release characteristics indicated that some CUR molecules were adsorbed onto the particle surface, while the sustained release characteristics suggested the diffusion of CUR

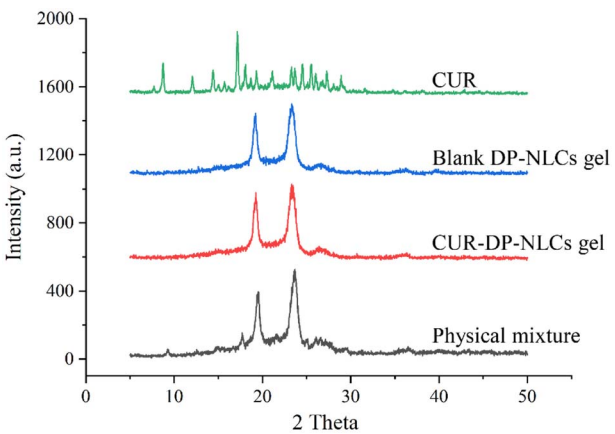

Fig. 3 XRD spectra of CUR, blank DP–NLCs gel, CUR–DP–NLCs gel and physical mixture.

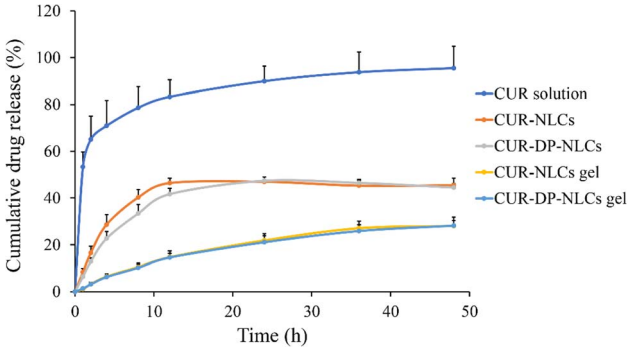

Fig. 4 *In vitro* CUR release of CUR solution, CUR–NLCs, CUR–DP–NLCs, CUR–NLCs gel and CUR–DP–NLCs gel ($n = 3$).

from the core of the lipid matrix.[38] In addition, the drug release rate of CUR–DP–NLCs slightly decreased after surface modification in comparison to CUR–NLCs. The slowest CUR release profiles were observed in CUR–NLCs gel and CUR–DP–NLCs gel. Before released into the medium, CUR had to go through the nanostructure core and 3D network structure imparted by the F127 hydrogel, which obviously slowed down the release rate. This could protect CUR molecules from degradation, enhance the stability of the system and benefit to persistent topical therapy.[39]

3.7. *In vitro* skin permeation and retention

The *in vitro* skin permeation profiles of CUR from CUR solution, CUR–NLCs gel and CUR–DP–NLCs gel *versus* time were shown in Fig. 5A. It could be observed that the cumulative permeated amount of CUR from CUR–NLCs gel and CUR–DP–NLCs gel was higher than that from CUR solution at each experimental time point. After 24 h of topical administration, the cumulative permeation of CUR in the CUR–NLCs gel and the CUR–DP–NLCs gel groups were, respectively, 3.02- and 2.37-fold higher than that in the CUR solution group. According to the early reports, it could be concluded that NLC gel ensured close contact with stratum corneum and increased the amount of encapsulated drug penetrating into the skin, profiting from occlusive effect and film formation on the skin surface of NLC.[14] Despite the hydrophilic character of the gel, the high lipid content dispersed therein could lead to an occlusive effect that prevented the loss of transepidermal water and increased skin hydration, promoting the penetration of drugs into the skin.[16] In addition, the physiological lipid composition of NLC could interact with the stratum corneum, creating skin lipids rearrangement, which facilitated drug penetration.[40]

After 24 h *in vitro* permeation experiments, the amounts of CUR deposited in the skin samples were determined and the result was depicted in Fig. 5B. The drug retained in the skin of CUR–DP–NLCs gel was significantly higher ($p < 0.05$) than that of CUR–NLCs gel and CUR solution. The deposition amount of CUR–DP–NLCs gel was 2.14-fold higher than that of CUR–NLCs gel and 2.85-fold higher than that of CUR solution, respectively. The enhanced skin retention of CUR–DP–NLCs gel for topical delivery might be attributed to several factors: (i) NLC nanoparticles were capable of forming a drug reservoir in the skin, which prolonged the retention time of drug in the skin so as to ensure the lasting and slow release of drug.[14] (ii) The average particle size of the modified CUR–DP–NLCs was larger than that of the non-modified NLCs, which might contribute to remain in the local skin layers.[40] (iii) It was postulated that acetyl dipeptide-1 cetyl ester interacted with the TRPV1 channel expressed on keratinocytes and sebocytes in skin tissues, resulting in the retention of CUR–DP–NLC in the skin.[21] The results revealed that CUR–DP–NLC gel could increase the skin retention and decrease further permeation of CUR which indicate maximum efficacy in targeted localized skin part with minimal systemic loss.[41]

3.8. Fluorescence microscopy imaging

The *in vivo* skin penetration of nanoparticles was tracked by fluorescence microscopy. Fig. 6 depicted the fluorescent microscopy images of vertical skin sections obtained 1 h and 6 h

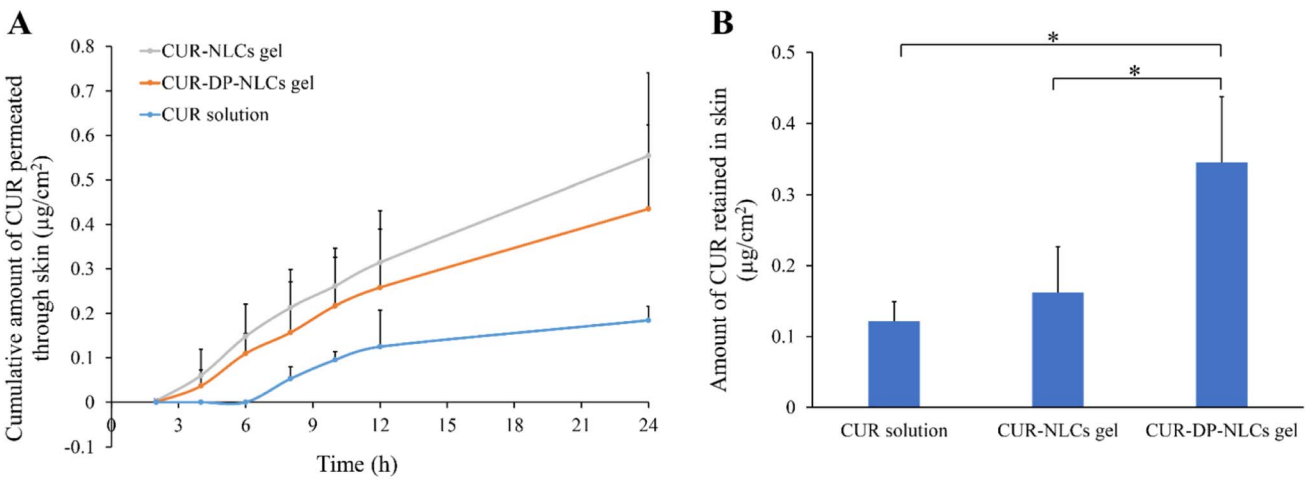

Fig. 5 (A) *In vitro* skin permeation profiles of CUR from CUR solution, CUR–NLCs gel and CUR–DP–NLCs gel. (B) CUR retention in rat skins after exposure to CUR solution, CUR–NLCs gel and CUR–DP–NLCs gel for 24 h. Results were presented as mean ± SD ($n = 3$; *$p < 0.05$).

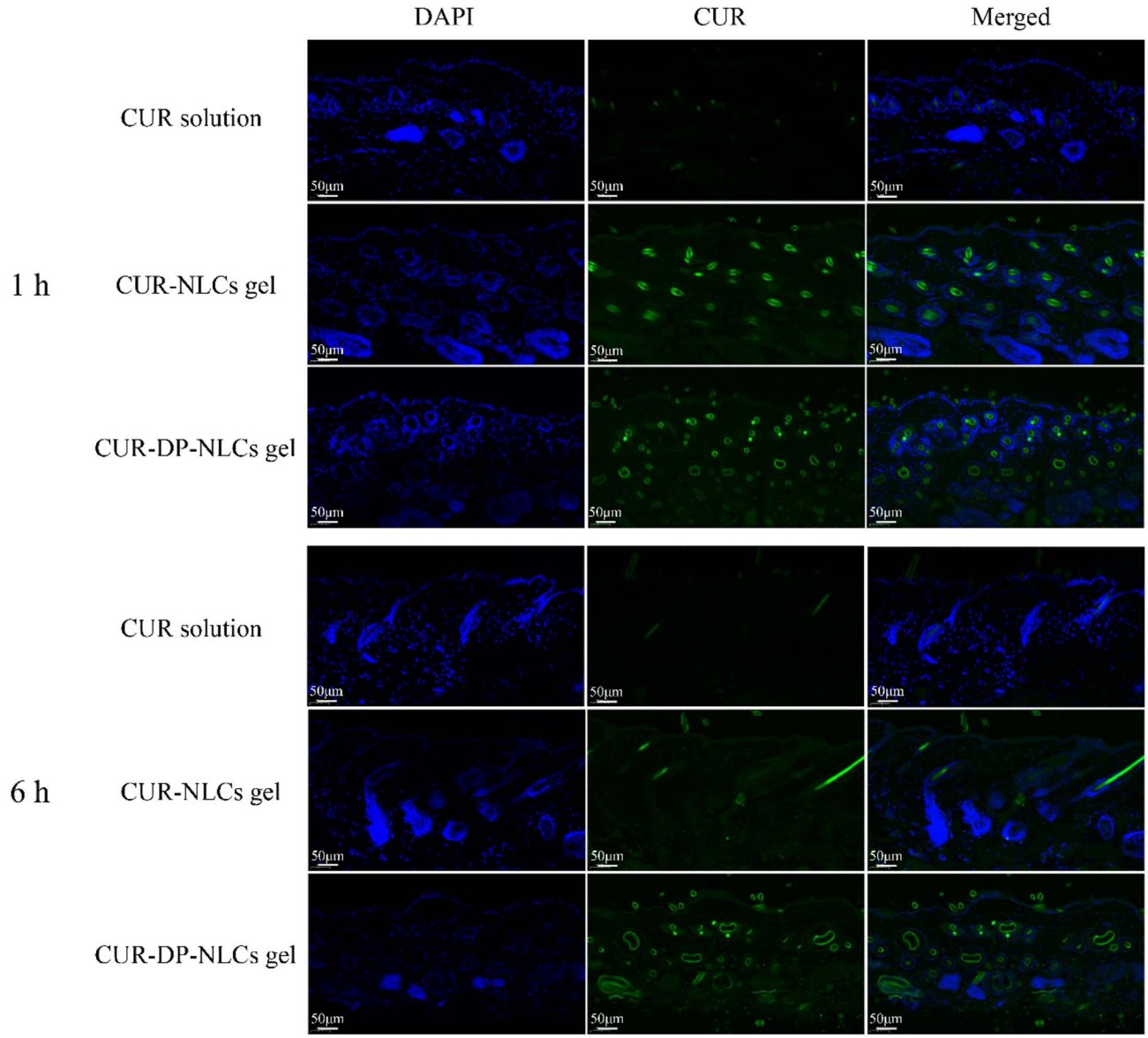

Fig. 6 Fluorescence images of longitudinal skin sections after the mice were treated with CUR solution, CUR–NLCs gel and CUR–DP–NLCs gel for 1 h and 6 h (scale bar: 50 μm).

after the application of CUR solution, CUR–NLCs gel and CUR–DP–NLCs gel. For the CUR solution group, no strong fluorescent signal was observed in the hair follicles of the skin samples at all the predetermined time points, indicating its poor permeability of CUR molecules. After 1 h of administration, both the CUR–NLCs gel and CUR–DP–NLCs gel groups showed strong green autofluorescence in the skin indicative of CUR, confirming NLCs were capable of crossing the stratum corneum, reaching the epidermis and dermis. It was observed that CUR did not homogeneously cover the skin, but accumulated in hair follicles, which indicated that NLC nanoparticles could penetrate faster through hair follicles than other routes.[42] The CUR fluorescence of CUR–NLCs gel group obviously decreased compared with that of CUR–DP–NLCs gel 6 h after application. The results demonstrated the superiority of CUR–DP–NLCs gel for topical CUR delivery, and CUR–DP–NLC nanoparticles accumulated in the hair follicles, forming a reservoir from which they could release the drug.[43]

3.9. Histological analysis

The effects of the formulations on the microstructure of skin were studied by histological analysis and examined microscopically using hematoxylin–eosin (HE) staining as depicted in Fig. 7. In the normal saline group, the skin structure was complete and skin stratification was clear. The stratum corneum layer was intact and epidermis layer was tightly arranged, with the corneocytes closely connected. After treatment with CUR solution, the intercellular space slightly increased and the skin layers were still clear. In contrast, the skin structure of CUR–NLCs gel and CUR–DP–NLCs gel groups changed

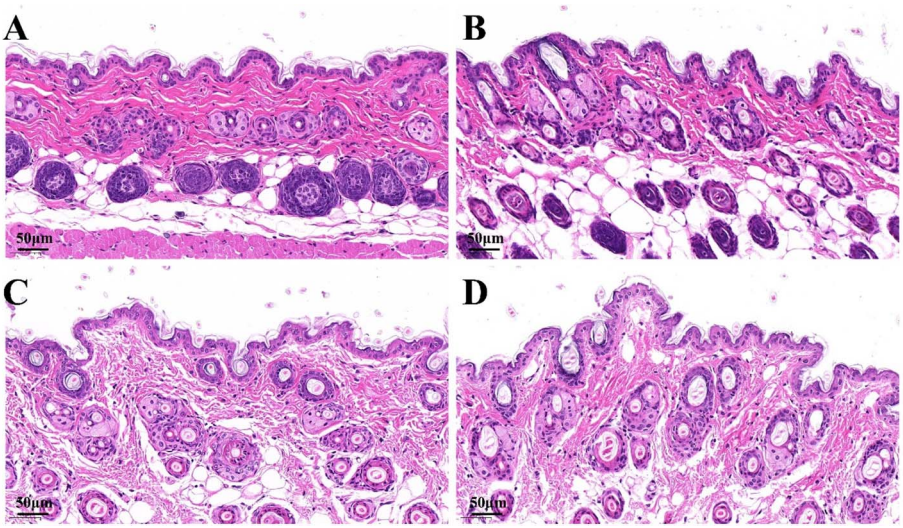

Fig. 7 Micrographs of HE-stained skin sections after the mice were treated with saline (A), CUR solution (B), CUR–NLCs gel (C) and CUR–DP–NLCs gel (D) for 6 h (scale bar: 50 μm).

markedly. The stratum corneum was loose and thin, the intercellular space further increased, and the corneocytes were loosely arranged. This might be attributed to the occlusive film formed by NLC nanoparticles at skin surface, which prevented transepidermal water loss and promoted skin hydration, generating a more loose packing on both corneocytes and lipids. Moreover, the surfactants used as stabilizers of NLC might interact with the components of the skin, causing the skin structure disruption and increasing the lipid nanoparticles diffusion.[43]

Table 2 Topical anti-inflammatory activity on xylene-induced ear edema in mice. The data was represented as mean ± SD ($n = 8$)[a]

Groups	Extent of edema (mg)	Inhibition (%)
Saline	25.6 ± 7.2	—
Blank gel	26.2 ± 6.3	—
CUR solution	24.2 ± 7.9	5.47
CUR–NLCs gel	20.5 ± 7.0	19.92
CUR–DP–NLCs gel	17.9 ± 4.2*#	30.08

[a] The data was represented as mean ± SD ($n = 8$); *$p < 0.05$ *vs.* saline group, #$p < 0.05$ *vs.* blank gel group.

3.10. Anti-inflammatory activity evaluation

The anti-inflammatory action of different formulations on xylene-induced mouse ear edema was presented in Table 2. As shown in the Table 2, CUR–DP–NLCs gel significantly reduced the ear edema caused by xylene compared to saline group ($p < 0.05$). The ear edema inhibition of CUR–DP–NLCs gel group was 5.50- and 1.51-fold higher than that of CUR solution and CUR–NLCs gel groups, respectively. This could be ascribed to increased CUR concentration deposited in the skin treated with CUR–DP–NLCs gel. Moreover, acetyl dipeptide-1 cetyl ester might inhibit neurogenic inflammation in skin and reduce prostaglandin E2 (PGE_2) secretion and decrease nuclear factor κB (NFκB) signaling. The results suggested a potential therapeutic implication of CUR–DP–NLCs gel on topical inflammatory skin.[19,20]

3.11. Analgesic activity evaluation

The analgesic activity of different formulations was assessed using the hot plate method and the results of mean mice reaction time towards thermal stimulus pain were represented in Table 3. It was observed that CUR–DP–NLCs gel group showed a significant prolonged reaction time ($p < 0.05$) that began at 1 h and lasted up until 2 h after treatment, in

Table 3 The pain reaction time of mice subjected to the hot plate test. The data was represented as mean ± SD ($n = 8$)[a]

		Reaction time (s)		
Groups	Pre-treatment (s)	0.5 h	1 h	2 h
Saline	18.15 ± 5.32	16.32 ± 6.68	19.32 ± 8.24	19.18 ± 5.31
Blank gel	18.92 ± 6.03	17.96 ± 4.95	18.11 ± 7.56	17.36 ± 7.95
CUR solution	18.56 ± 4.71	21.63 ± 5.99	21.88 ± 8.02	22.86 ± 6.77
CUR–NLCs gel	19.41 ± 4.81	21.13 ± 5.96	24.55 ± 8.28	24.09 ± 8.69
CUR–DP–NLCs gel	19.46 ± 5.76	20.78 ± 7.83	28.89 ± 6.22*#	31.36 ± 7.66*#$

[a] The data was represented as mean ± SD ($n = 8$); *$p < 0.05$ *vs.* saline group, #$p < 0.05$ *vs.* blank gel group, $$p < 0.05$ *vs.* CUR solution group.

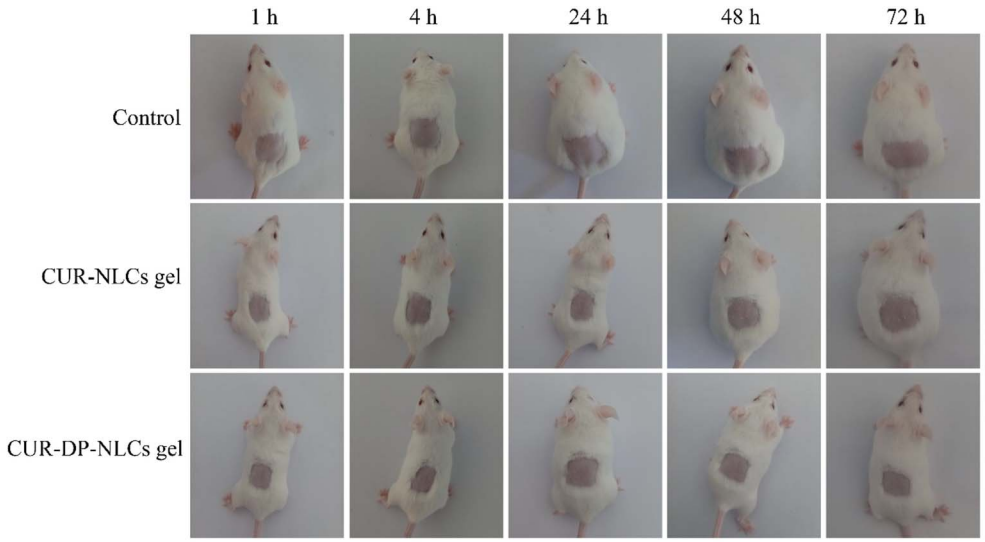

Fig. 8 Skin appearance of mice observed at 1, 4, 24, 48 and 72 h after removing the residual formulation.

comparison to the saline and blank gel groups. The longest time responses of CUR–NLCs gel and CUR–DP–NLCs gel groups were, respectively, 24.09 s and 31.36 s at 2 h after topical administration, and CUR–DP–NLCs gel appeared to induce higher analgesic effect.

3.12. *In vivo* skin irritation study

Skin irritation study was performed to assess the potential influence of the formulations on skins. As shown in Fig. 8, neither CUR–NLCs gel nor CUR–DP–NLCs gel triggered skin irritation, compared to the saline group (control). No signs of erythema or edema were observed in the application site within overall 72 h of the experiment. These results advocated that the developed NLC hydrogels were well-tolerated and supported the safeness of CUR–DP–NLCs gel for topical application.

4. Conclusions

In the present work, we have developed CUR–DP–NLCs gel as a novel topical drug carrier for CUR. The CUR–DP–NLCs were spherical, uniformly nanosized, and showed an adequate zeta potential and high EE. It was indicated that CUR–DP–NLCs gel had a sustained release profile and could enhance drug retention in skins compared with unmodified NLCs gel. CUR–DP–NLCs gel could accumulate in the hair follicles and enable prolong the retention in the site of action. Furthermore, CUR–DP–NLCs gel also induced higher anti-inflammation and analgesic effect after topical administration. In summary, CUR–DP–NLCs gel could be considered as a kind of promising preparation for treatment of topical pain and skin inflammation.

Ethical statement

The animals were acclimatised at regulated temperature (20 ± 5 °C) and humidity ($50 \pm 5\%$) under natural light/dark conditions for at least 1 week before experimentation, fed with a standard diet and allowed water *ad libitum*. The experimental protocols were in accordance with the guidelines approved by Luoyang Normal University, and the study was approved by the Experimental Animal Ethics Committee.

Conflicts of interest

The authors declare no conflict of interest.

Acknowledgements

This work was supported by the Key Scientific Research Project of Higher Education of Henan Province (No. 23A350002), the National Project Cultivation Fund of Luoyang Normal University (No. 2019-PYJJ-012), the Key Scientific and Technological Project of Henan of China (No. 232102311164), the Innovative Training Program for College Students in Henan Province of China (No. 202310482004 and No. 202310482008).

References

1 M. Zatorska-Plachta, G. Lazarski, U. Maziarz, A. Forys, B. Trzebicka, D. Wnuk, K. Choluj, A. Karewicz, M. Michalik, D. Jamroz and M. Kepczynski, *ACS Omega*, 2021, **6**, 12168–12178.
2 M. S. Algahtani, M. Z. Ahmad, I. H. Nourein and J. Ahmad, *Biomolecules*, 2020, **10**, 968.
3 L. Vollono, M. Falconi, R. Gaziano, F. Iacovelli, E. Dika, C. Terracciano, L. Bianchi and E. Campione, *Nutrients*, 2019, **11**, 2169.
4 J. A. Luckanagul, P. R. Na Bhuket, C. Muangnoi, P. Rojsitthisak, Q. Wang and P. Rojsitthisak, *Polymers*, 2021, **13**, 194.
5 V. Campani, L. Scotti, T. Silvestri, M. Biondi and G. De Rosa, *J. Mater. Sci.: Mater. Med.*, 2020, **31**, 18.

6 T. Jiang, T. Wang, T. Li, Y. Ma, S. Shen, B. He and R. Mo, *ACS Nano*, 2018, **12**, 9693–9701.
7 J. Niu, M. Yuan, Y. Liu, L. Wang, Z. Tang, Y. Wang, Y. Qi, Y. Zhang, H. Ya and Y. Fan, *Front. Chem.*, 2022, **10**, 1028372.
8 Y. Zhang, Q. Xia, Y. Li, Z. He, Z. Li, T. Guo, Z. Wu and N. Feng, *Theranostics*, 2019, **9**, 48–64.
9 A. A. Vigato, S. M. Querobino, N. C. de Faria, A. Candido, L. G. Magalhaes, C. M. S. Cereda, G. R. Tofoli, E. V. R. Campos, I. P. Machado, L. F. Fraceto, M. I. de Sairre and D. R. de Araujo, *Front. Pharmacol*, 2019, **10**, 1006.
10 S. Ahmed, S. Mahmood, M. Danish Ansari, A. Gull, N. Sharma and Y. Sultana, *Int. J. Pharm.*, 2021, **607**, 121006.
11 P. S. Rajinikanth and J. Chellian, *Int. J. Nanomed.*, 2016, **11**, 5067–5077.
12 L. Miao, L. Daozhou, C. Ying, M. Qibing and Z. Siyuan, *Colloids Surf., B*, 2021, **204**, 111786.
13 S. Khurana, N. K. Jain and P. M. Bedi, *Life Sci.*, 2013, **93**, 763–772.
14 F. Han, R. Yin, X. Che, J. Yuan, Y. Cui, H. Yin and S. Li, *Int. J. Pharm.*, 2012, **439**, 349–357.
15 S. Jain, R. Addan, V. Kushwah, H. Harde and R. R. Mahajan, *Int. J. Pharm.*, 2019, **562**, 96–104.
16 I. T. Mendes, A. L. M. Ruela, F. C. Carvalho, J. T. J. Freitas, R. Bonfilio and G. R. Pereira, *Colloids Surf., B*, 2019, **177**, 274–281.
17 K. Fang, R. Wang, H. Zhang, L. Zhou, T. Xu, Y. Xiao, Y. Zhou, G. Gao, J. Chen, D. Liu, F. Ai and J. Fu, *ACS Appl. Mater. Interfaces*, 2020, **12**, 52307–52318.
18 Y. Huang, S. Qian, J. Zhou, W. Chen, T. Liu, S. Yang, S. Long and X. Li, *Adv. Funct. Mater.*, 2023, **33**, 2213549.
19 D. Resende, M. S. Ferreira, J. M. Sousa-Lobo, E. Sousa and I. F. Almeida, *Pharmaceuticals*, 2021, **14**, 702.
20 M. S. Ferreira, J. M. S. Lobo and I. F. Almeida, *Int. J. Cosmet. Sci.*, 2022, **44**, 56–73.
21 M. Sulzberger, A. C. Worthmann, U. Holtzmann, B. Buck, K. A. Jung, A. M. Schoelermann, F. Rippke, F. Stab, H. Wenck, G. Neufang and E. Gronniger, *J. Eur. Acad. Dermatol. Venereol.*, 2016, **30**(suppl. 1), 9–17.
22 J. Luan, D. Zhang, L. Hao, L. Qi, X. Liu, H. Guo, C. Li, Y. Guo, T. Li, Q. Zhang and G. Zhai, *Colloids Surf., B*, 2014, **114**, 255–260.
23 R. d. M. Barbosa, L. N. M. Ribeiro, B. R. Casadei, C. M. G. da Silva, V. A. Queiroz, N. Duran, D. R. de Araujo, P. Severino and E. de Paula, *Pharmaceutics*, 2018, **10**, 231.
24 Z. Teng, M. Yu, Y. Ding, H. Zhang, Y. Shen, M. Jiang, P. Liu, Y. Opoku-Damoah, T. J. Webster and J. Zhou, *Int. J. Nanomed.*, 2019, **14**, 119–133.
25 J. Niu, M. Yuan, Z. Zhang, L. Wang, Y. Fan, X. Liu, X. Liu, H. Ya, Y. Zhang and Y. Xu, *Int. J. Nanomed.*, 2022, **17**, 4009–4022.
26 L. M. Tunin, F. B. Borghi, A. C. Nogueira, L. Higachi, D. S. Barbosa, M. L. Baesso, L. Hernandes, A. Diniz and M. d. C. Truiti, *Pharm. Biol.*, 2016, **54**, 139–145.
27 M. H. Abdallah, A. S. Abu Lila, R. Unissa, H. S. Elsewedy, H. A. Elghamry and M. S. Soliman, *Colloids Surf., B*, 2021, **205**, 111868.
28 N. Righi, S. Boumerfeg, A. Deghima, P. A. R. Fernandes, E. Coelho, F. Baali, S. M. Cardoso, M. A. Coimbra and A. Baghiani, *J. Ethnopharmacol.*, 2021, **272**, 113940.
29 S. H. Nam, Y. J. Xu, H. Nam, G. W. Jin, Y. Jeong, S. An and J. S. Park, *Int. J. Pharm.*, 2011, **419**, 114–120.
30 P. Carter, B. Narasimhan and Q. Wang, *Int. J. Pharm.*, 2019, **555**, 49–62.
31 Y. Zhang, W. Ng, J. Hu, S. S. Mussa, Y. Ge and H. Xu, *Colloids Surf., B*, 2018, **163**, 184–191.
32 T. Moqejwa, T. Marimuthu, P. P. D. Kondiah and Y. E. Choonara, *Pharmaceutics*, 2022, **14**, 703.
33 M. Liu, F. Wang, C. Pu, W. Tang and Q. Sun, *Food Chem.*, 2021, **358**, 129840.
34 E. L. de Oliveira, S. B. S. Ferreira, L. V. de Castro-Hoshino, K. Campanholi, I. R. Calori, F. A. P. de Morais, E. Kimura, R. C. da Silva Junior, M. L. Bruschi, F. Sato, N. Hioka and W. Caetano, *Langmuir*, 2021, **37**, 3202–3213.
35 P. Liu, H. Shen, Y. Zhi, J. Si, J. Shi, L. Guo and S. G. Shen, *Colloids Surf., B*, 2019, **181**, 1026–1034.
36 E. S. Behbahani, M. Ghaedi, M. Abbaspour and K. Rostamizadeh, *Ultrason. Sonochem.*, 2017, **38**, 271–280.
37 R. S. Mulik, J. Monkkonen, R. O. Juvonen, K. R. Mahadik and A. R. Paradkar, *Int. J. Pharm.*, 2010, **398**, 190–203.
38 A. R. Neves, M. Lucio, S. Martins, J. L. Lima and S. Reis, *Int. J. Nanomed.*, 2013, **8**, 177–187.
39 D. Liu, J. Li, H. Pan, F. He, Z. Liu, Q. Wu, C. Bai, S. Yu and X. Yang, *Sci. Rep.*, 2016, **6**, 28796.
40 A. Garces, M. H. Amaral, J. M. Sousa Lobo and A. C. Silva, *Eur. J. Pharm. Sci.*, 2018, **112**, 159–167.
41 V. K. Rapalli, V. Kaul, T. Waghule, S. Gorantla, S. Sharma, A. Roy, S. K. Dubey and G. Singhvi, *Eur. J. Pharm. Sci.*, 2020, **152**, 105438.
42 K. Krambeck, V. Silva, R. Silva, C. Fernandes, F. Cagide, F. Borges, D. Santos, F. Otero-Espinar, J. M. S. Lobo and M. H. Amaral, *Int. J. Pharm.*, 2021, **600**, 120444.
43 M. A. Espinosa-Olivares, N. L. Delgado-Buenrostro, Y. I. Chirino, M. A. Trejo-Marquez, S. Pascual-Bustamante and A. Ganem-Rondero, *Eur. J. Pharm. Sci.*, 2020, **155**, 105533.